

Soft-clamped silicon nitride string resonators at millikelvin temperatures

Thomas Gisler,¹ Mohamed Helal,¹ Deividas Sabonis,¹ Urs Grob,¹ Martin H eritier,¹ Christian L. Degen,¹ Amir H. Ghadimi,^{2,*} and Alexander Eichler^{1,†}

¹Laboratory for Solid State Physics, ETH Z urich, 8093 Z urich, Switzerland.

²Centre Suisse d'Electronique et de Microtechnique SA (CSEM), 2002 Neuch atel, Switzerland.

We demonstrate that soft-clamped silicon nitride strings with large aspect ratio can be operated at mK temperatures. The quality factors (Q) of two measured devices show consistent dependency on the cryostat temperature, with soft-clamped mechanical modes reaching $Q > 10^9$ at roughly 46 mK. For low optical readout power, Q is found to saturate, indicating good thermalization between the sample and the stage it is mounted on. Our best device exhibits a calculated force sensitivity of $9.6 \text{ zN}/\sqrt{\text{Hz}}$ and a thermal decoherence time of 0.38 s, which bode well for future applications such as nanomechanical force sensing.

Over the last years, string and membrane micromechanical resonators made from high-stress silicon nitride (Si_3N_4) have established themselves as a powerful system for quantum engineering [1–7]. Applications range from electro-opto-mechanical transduction of quantum states [8, 9] to scanning force microscopy [10], nuclear spin imaging [11, 12], spin-phonon entanglement [13, 14], and gravitational wave detection [15]. These applications profit immensely from cryogenic cooling of the resonator, both due to the lower thermomechanical noise and because the mechanical quality factor Q generally increases with reduced temperatures [16, 17].

Even though Si_3N_4 resonators are expected to achieve their best performance at millikelvin temperatures, little is known about their actual properties (intrinsic Q , thermal conductivity, Young's modulus, ...) under such conditions [16, 18], in particular in the presence of optical absorption [15, 17]. This is in part owed to the technical difficulties added by working in a dry dilution refrigerator, whose vibrations can furthermore add force and frequency noise [19]. More fundamental, however, is a concern that the interaction with an optical light field will induce heating in the mechanical device, making it difficult to consistently operate at mK temperatures. This issue could be strong for one-dimensional (string) devices [7, 20, 21], whose extreme aspect ratio is expected to lead to inefficient heat conduction.

In this work, we experimentally demonstrate that a corrugated soft-clamped Si_3N_4 string resonator with an aspect ratio of 200 000 (4 mm long, 20 nm thick) can be operated at temperatures as low as $46 \pm 10 \text{ mK}$. We cool the strings in a dry dilution refrigerator with a custom-built vibration isolation and a compact optical interferometer readout that allows us to characterize the resonator decay times during ringdown experiments. Through careful analysis, we infer that the string achieves thermal equilibrium with the sample plate for low optical readout power. Our best device reaches a mean value for the quality factor of $(2.3 \pm 0.12) \times 10^9$ at a resonance fre-

quency of 1.406 MHz, corresponding to an intrinsic force sensitivity of $9.6 \text{ zN}/\sqrt{\text{Hz}}$ and a dissipation-limited coherence time of 0.38 s. Our work further shows a strong increase of Q at the lowest measured temperatures, providing fresh insight regarding the fundamental limitations of the coherence of mechanical state.

We study soft-clamped nanostrings made from prestressed Si_3N_4 [6], see Fig. 1(a). The fabrication procedure is detailed in the Supplemental Material. The devices are mounted in a Leiden CF450 dilution refrigerator with a mixing chamber base temperature of approximately $T_{\text{mc}} = 30 \text{ mK}$, corresponding to a sample plate temperature as low as $T_{\text{plate}} = 40 \text{ mK}$ [22–24]. A spring suspension with soft copper braids between the mixing chamber and the sample stage reduces the in-coupling of mechanical noise. Two heaters at the sample stage allow for variations of the sample plate temperature between 46 and 194 mK.

Mechanical oscillations of the string are measured with a fiber-based optical interferometer, see Fig. 1(b) [23, 25]. A piezoelectric actuator excites mechanical oscillations to the initial amplitude used for ringdown measurements. To reduce optical heating and back-action effects, we apply a stroboscopic measurement scheme [6] as shown in Fig. 1(c). A variable optical attenuator turns the illumination of the device on and off, enabling “ringdowns in the dark” whose progress is only intermittently probed. The photo current from the signal diode is amplified and measured with a lock-in detector. A phase-locked loop (PLL) is used to continuously adjust the local oscillator frequency of the lock-in amplifier to the mechanical resonance frequency during each ‘on’ period.

Corrugated nanostrings exhibit a distinctive mode structure which is dictated by the number of unit cells and their geometry. The periodic corrugation creates a phononic crystal (PnC) with a bandgap [20]. This bandgap spatially confines certain flexural modes, whose quality factors are enhanced due to a reduction in the clamping loss, see Fig. 2(a) [5, 20, 26]. For our initial study, we use a 4 mm-long and 100 nm-thick string, with a width varying between $w_{\text{min}} = 500 \text{ nm}$ and $w_{\text{max}} = 1200 \text{ nm}$ (Device A, see Table. I). For the particular string studied here, the soft-clamped mode has a resonance fre-

* Corresponding author: amir.ghadimi@csem.ch

† Corresponding author: eichlera@ethz.ch

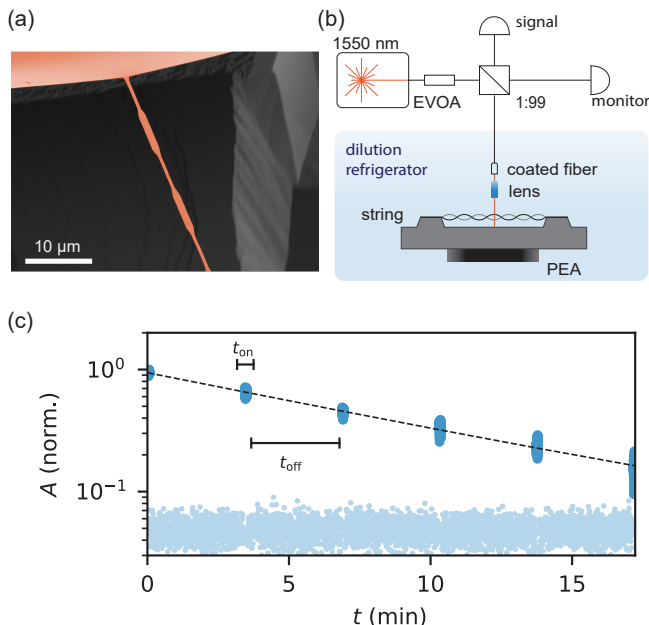


FIG. 1. Experimental setup and stroboscopic ring-down. (a) A false-colored SEM image of a string device similar to the ones used in this study. Shown is one clamping point and two unit cells. (b) Schematic illustration of the setup: A 1550 nm laser is used to measure the displacement of the Si_3N_4 beam. An electronic variable optical attenuator (EVOA) is used to switch on and off the optical readout for the stroboscopic measurements. The light reflected from the device interferes with the light reflected at the semi-transparent coated fiber end. The light is focused with a gradient-index (GRIN) lens. The resonator motion is excited via a piezoelectric actuator (PEA) attached to the sample holder. The ac photo detector signal is recorded with a lock-in amplifier. (c) Stroboscopic ringdown measurement of the localized mode with frequency $f_0 = 1.406$ MHz at $T_{\text{plate}} = 46$ mK with $t_{\text{on}} = 5$ s and $t_{\text{off}} = 200$ s. The best fit for this particular ringdown yields $Q = 2.41 \pm 0.05 \times 10^9$ (95% confidence interval of the fit). Roughly 120 nW of laser power were focused on the resonator with a duty cycle of 0.02, yielding an average power of 2.4 nW.

quency of $f_{\text{loc}} = 1.237$ MHz at room temperature, well inside the phononic bandgap indicated by a shaded region in Fig. 2(b). The effect of soft-clamping for the in-bandgap mode is clearly visible, since only this mode exceeds $Q > 10^7$.

Frequencies as well as quality factors of the mechanical modes are affected by changes in temperature. While the relative changes in frequency are small (e.g. $\delta f_{\text{loc}} = 20$ kHz for a localized mode with $f_{\text{loc}} = 1.237$ MHz), the quality factors increase significantly. In Fig. 2(b), we observe a consistent increase of the quality factors at 4 K compared to room temperature for all modes.

The stress, and therefore the dissipation dilution factor of pre-stressed resonators, increases for reduced beam cross sections [5, 6]. In order to achieve higher quality factors, we repeat the measurements with two 20 nm-

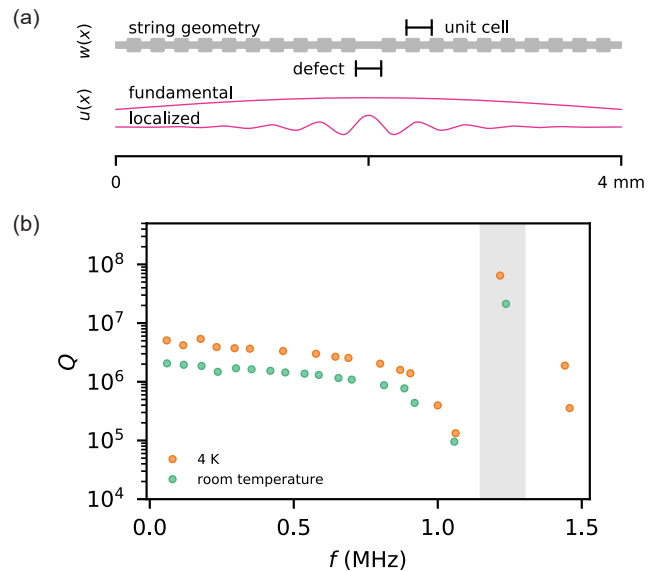


FIG. 2. String geometry and mode structure of device A. (a) Shape $w(x)$ of the 4 mm long corrugated beam with 10 unit cells on each side ($n = 10$) with a unit cell pitch of 100 μm , filling factor of 50% ($w_{\text{min}} = 500$ nm, $w_{\text{max}} = 1200$ nm), and a defect at the center with a width of 500 nm and length of 120 μm . The corresponding fundamental and localized mode shapes are shown as $u(x)$. (b) Quality factors of various mechanical modes of the corrugated string at room temperature (green) and at 4 K (orange). The string is 100 nm thick and grey shading indicates the extent of the phononic bandgap.

	Device A	Device B	Device C
Length	4 mm	4 mm	4 mm
Thickness	100 nm	20 nm	20 nm
Unit cells	10	12	12
D-to-UC ratio	1.2	1.1	1.2
f_{loc}	1.237 MHz	1.443 MHz	1.406 MHz
$Q_{300} (\times 10^6)$	21	73	100
$Q_4 (\times 10^6)$	65	540	730
$Q_{46\text{m}} (\times 10^6)$		1600	2300

TABLE I. List of devices. The temperature for the Q_4 is between 4 and 7 K. D-to-UC ratio is the ratio between the length of the defect and the pitch of a unit cell as indicated in Fig. 2(a).

thick strings. We investigate strings with 12 unit cells, with defect-to-unit-cell (D-to-UC) ratios of 1.1 (device B) and 1.2 (device C). The frequencies of the fundamental modes are $f_1^{\text{B(C)}} = 56.6$ kHz (56.3 kHz) and those of the localized mode (mode number 25) are $f_{\text{loc}}^{\text{B(C)}} = 1.443$ MHz (1.406 MHz) at room temperature.

Figure 3 summarizes the Q values we measured for the fundamental and localized modes of the two devices B and C over the full temperature range. The localized modes show a constant and roughly ten-fold higher quality factor compared to the fundamental modes, while the

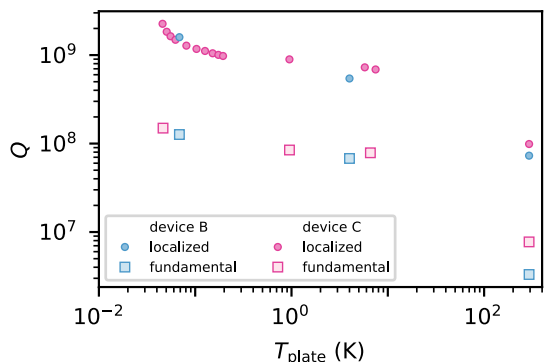


FIG. 3. **Quality factor for various temperatures.** Measured Q of two 20 nm-thick strings with $n = 12$ unit cells and different defect-to-unit-cell ratio (device B: ratio 1.1, blue, device C: ratio 1.2, red) at various temperatures. For each string, circles and squares correspond to the localized and fundamental modes, respectively.

variations between the two devices are small. A reduction of the temperature from room temperature to 4 K leads to an improvement of all quality factor values by a factor ~ 10 . Further cooling to the base temperature of the refrigerator ($T_{\text{mc}} = 30$ mK) leads to another steep increase of Q for the localized mode of device C reaching up to $Q = 2 \times 10^9$. The heating experiment has exclusively been conducted with device C. A similar increase has been reported for metal-coated silicon strings [27] and with silicon nitride membrane resonators [15–18], but its microscopic origin remains unclear. To confirm the validity of our result, we performed careful studies as a function of average optical power and sample plate temperature that we present in the following. We note that the thermometer installed on the sample plate was not operational during these experiments. The temperature values reported here are the result of a careful calibration study between T_{plate} and T_{mc} that we performed in an additional cooldown. The calibration is shown in the supplemental material [24].

The interaction of the string with the laser beam can induce two effects in the resonator modes: (i) on the one hand, optical absorption heats up the string above the lattice temperature of the stage it is mounted on. (ii) On the other hand, radiation pressure forces or photothermal forces act as positive or negative feedback that drive or damp a resonator mode [28, 29]. To minimize these effects, we employ stroboscopic ringdown measurements, where light illuminates the string only for short periods t_{on} between ‘dark’ periods t_{off} (see Fig. 1(c)). The duty cycle D of a stroboscopic measurement is defined as $D = t_{\text{on}}/(t_{\text{on}} + t_{\text{off}})$. We repeat ringdown measurements for positive and negative optical damping to characterize the influence of optomechanical feedback forces (cf. SM [24] for details regarding the fringe structure).

In Fig. 4(a), we see that the difference between opposite feedback forces is small. This indicates that the

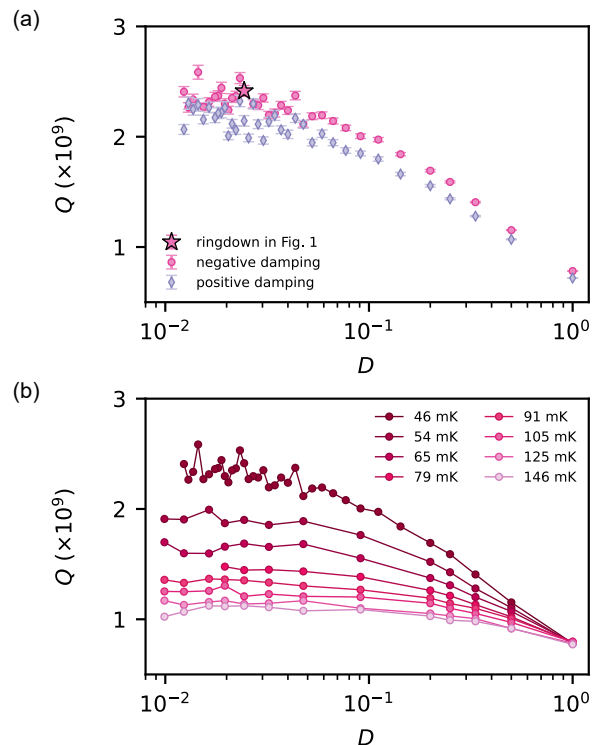


FIG. 4. **Quality factor dependence on laser duty cycle and temperature.** (a) Quality factor of device C as a function of the duty cycle D of the laser in the stroboscopic measurement. We kept $t_{\text{on}} = 5$ s and varied t_{off} . Since the beam waist is larger than the string width, only around 120 nW of the 1.3 μ W incident laser power is focused on the string while the laser is on. The interferometer is locked to values that induce either positive and negative damping (cf. SM [24]). Error bars corresponds to 95% confidence interval of the best fit. (b) Q of device C for increasing sample plate sensor temperatures T_{plate} .

influence of radiation pressure or photo-thermal forces is minor. In contrast, the measured quality factor depends strongly on the duty cycle D , i.e., the average heating power arriving on the string surface. The effect is strongest when operating at the base temperature of the cryostat. The quality factor increases as we reduce D and plateaus for $D < 0.03$. This suggests that in this regime (i) either the string is well thermalized with the sample plate and the laser-induced heating is negligible, or (ii) Q becomes independent of temperature below $T_{\text{plate}} \approx 200$ mK.

In Fig. 4(b), we show repeated measurements of Q as a function of D in the presence of a local heater mounted on the sample plate. Increasing T_{plate} leads to an immediate reduction of Q , demonstrating clearly that option (ii) is wrong. We therefore conclude that option (i) is correct: our string resonators do thermalize with the sample plate temperature T_{plate} .

One possible explanation of the reduced dissipation below 200 mK is the non-resonant coupling between ensem-

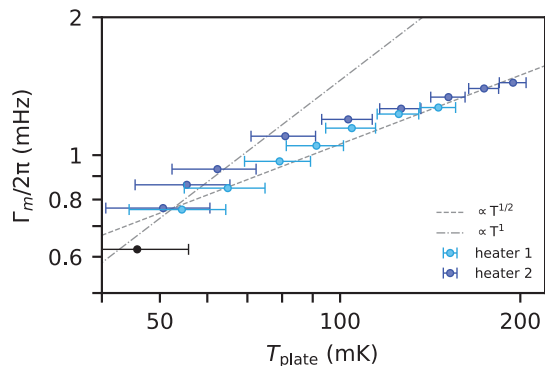


FIG. 5. **Temperature-dependent dissipation coefficient.** Γ_m measured as a function of T_{plate} with device C. Changes in T_{plate} were induced by two local heaters mounted on the sample stage (heater 1 and 2). The black dot corresponds to the case without heating. The dashed and dashed-dotted grey lines visualize the power laws $\Gamma_m \propto T^\nu$ with $\nu = 1/2$ [30] and $\nu = 1$ [31, 32] predicted by the STM for one-dimensional resonators. Error bars indicate the calibration uncertainty of 10 mK of the sample stage thermometer.

bles of defects in the material and the motion of the mechanical resonator [32]. The defects can be modelled as two-level systems (TLS) in an asymmetric double-well potential [31, 33]. The resonator oscillation induces localized strain variations that perturb the potential and couple the defects and phonons [34]. To compare our data to the standard tunnelling model (STM), we plot $\Gamma_m = 2\pi f_{\text{loc}}/Q$ as a function of T_{plate} in Fig. 5. Theoretical STM analyses on the role of TLS for nanomechanical resonators predict a power law $\Gamma_m \propto T^{1/2}$ [30] or $\Gamma_m \propto T$ [31, 32] for a quasi-one-dimensional string, with a plateau towards higher temperatures.

The comparison of experimental data to the STM has produced a variety of results in the past. With a range of different materials, measurements of quasi-one-dimensional devices were approximated as $\Gamma_m \propto T^\nu$ with $\nu = 1/3$ [35–37], $\nu = 2/3$ [38], or $\nu = 1$ [27, 32]. A saturation of Γ_m towards low temperatures was accounted for by the form $\Gamma_m \propto (1 + (T/T_0)^\nu)$, with the free parameters $T_0 = 0.3$ K and $\nu = 1.6$ [22, 30]. Our data shows a plateau of the dissipation above $T_{\text{plate}} \approx 150$ mK but no saturation at the lower end of the accessible temperature range.

The implications of our measurements remain to be investigated. In future work, we will study the possible presence of surface adsorbates that can introduce additional damping [39], and their partial desorption with strong local heaters [40].

Looking forward, high Q and low device temperatures are essential when using mechanical resonators for the detection of small forces. The nanostrings investigated in this work have a thermal noise-limited, single-sided

force sensitivity estimated as [41]

$$\sqrt{S_f} = \sqrt{4k_B T_{\text{plate}} m_{\text{eff}} \Gamma_m} = 9.6 \text{ zN}/\sqrt{\text{Hz}} \quad (1)$$

where k_B is the Boltzmann constant, $T_{\text{plate}} = 46$ mK is the device temperature, $\Gamma_m = 2\pi f_0/Q$ is the dissipation coefficient for a resonance frequency f_0 , and the effective mass $m_{\text{eff}} = 9.3$ pg is extracted from numerically solving the one-dimensional Euler-Bernoulli equation [26]. Our best device therefore attains a force sensitivity similar to that of a single carbon nanotube [42, 43], in spite of the roughly 10^6 times larger mass. In contrast to carbon nanotubes with a diameter of ≈ 1 nm, our top-down patterned Si_3N_4 strings are large enough to envisage mounting a molecular sample on them. This provides an interesting perspective for ultrasensitive force detection experiments, for instance in the context of nanoscale magnetic resonance imaging [12, 44–46]. A side-by-side comparison with the performance a state-of-the-art cantilever sensor confirms this assessment (cf. SM [24]).

Low temperatures and high quality factors are also important for increasing the quantum coherence time of the resonator’s oscillation states [18, 47]. Dissipation imposes a limit to the coherence time, yielding in our case

$$\gamma_{\text{diss}}^{-1} \approx \frac{1}{n\Gamma_m} = \frac{Q\hbar}{k_B T_{\text{plate}}} = 0.38 \text{ s} \quad (2)$$

where $n \approx 1000$ is the phonon occupation number of the resonator mode and \hbar is the reduced Planck constant. We emphasize, however, that frequency fluctuations [48] can significantly reduce this coherence time in practice. The characterization of frequency fluctuations in these corrugated string devices is an important topic to be explored in future studies.

A second crucial objective is to reduce the detection noise when reading out the nanomechanical oscillation. The simple interferometer used in the current setup is not optimized for string devices and produces significant additional readout noise, making the detection of thermomechanical force noise impossible. Integrated optomechanical readout [49, 50] can mitigate this problem. Increasing the vacuum optomechanical coupling rate g_0 [28] will allow better detection sensitivity for the same added heating. This is possible because the optomechanical cooperativity scales as G^2 , while absorption of light, in a rough approximation, is estimated to increase only linearly with G [51, 52].

In summary, we cooled and operated a Si_3N_4 string to a bath temperature of 46 mK, where it achieved a force sensitivity of $9.6 \text{ zN}/\sqrt{\text{Hz}}$ and a dissipation-limited coherence time of 0.38 s. We measure mechanical Q as high as 2.3×10^9 , more than $20\times$ improvement compared to room temperature. We observe a sudden increase of Q at the lowest temperatures of our dilution refrigerator, implying that further improvements should be achieved with a larger cooling power at base temperature and with better thermalization of the sample plate. The microscopic

origin of the damping and decoherence in our devices is not fully understood. However, the isolated nature of these localized modes provides an unique avenue for further work. Due to their simple geometry and strong isolation from environmental influences, nanomechanical

strings offer an ideal system to test model predictions.

ACKNOWLEDGMENTS

This work was supported by the Swiss National Science Foundation (CRSII5_177198/1) and an ETH Zurich Research Grant (ETH-51 19-2).

-
- [1] S. S. Verbridge, H. G. Craighead, and J. M. Parpia, A megahertz nanomechanical resonator with room temperature quality factor over a million, *Applied Physics Letters* **92**, 013112 (2008).
- [2] G. Anetsberger, E. Gavartin, O. Arcizet, Q. P. Unterreithmeier, E. M. Weig, M. L. Gorodetsky, J. P. Kotthaus, and T. J. Kippenberg, Measuring nanomechanical motion with an imprecision below the standard quantum limit, *Phys. Rev. A* **82**, 061804(R) (2010).
- [3] C. Reetz, R. Fischer, G. Assumpção, D. McNally, P. Burns, J. Sankey, and C. Regal, Analysis of membrane phononic crystals with wide band gaps and low-mass defects, *Physical Review Applied* **12**, 044027 (2019).
- [4] C. Reinhardt, T. Müller, A. Bourassa, and J. C. Sankey, Ultralow-noise sin trampoline resonators for sensing and optomechanics, *Phys. Rev. X* **6**, 021001 (2016).
- [5] Y. Tsaturyan, A. Barg, E. S. Polzik, and A. Schliesser, Ultracoherent nanomechanical resonators via soft clamping and dissipation dilution, *Nature Nanotechnology* **12**, 776 (2017).
- [6] A. H. Ghadimi, S. A. Fedorov, N. J. Engelsen, M. J. Beryhi, R. Schilling, D. J. Wilson, and T. J. Kippenberg, Elastic strain engineering for ultralow mechanical dissipation, *Science* **360**, 764 (2018).
- [7] A. Beccari, M. J. Beryhi, R. Groth, S. A. Fedorov, A. Arabmoheghi, N. J. Engelsen, and T. J. Kippenberg, Hierarchical tensile structures with ultralow mechanical dissipation (2021), [arXiv:2103.09785](https://arxiv.org/abs/2103.09785).
- [8] T. Bagci, A. Simonsen, S. Schmid, L. G. Villanueva, E. Zeuthen, J. Appel, J. M. Taylor, A. Sørensen, K. Usami, A. Schliesser, and E. S. Polzik, Optical detection of radio waves through a nanomechanical transducer, *Nature* **507**, 81 (2014).
- [9] R. W. Andrews, R. W. Peterson, T. P. Purdy, K. Cicak, R. W. Simmonds, C. A. Regal, and K. W. Lehnert, Bidirectional and efficient conversion between microwave and optical light, *Nature Physics* **10**, 321 (2014).
- [10] D. Hälgl, T. Gisler, Y. Tsaturyan, L. Catalini, U. Grob, M.-D. Krass, M. Héritier, H. Mattiat, A.-K. Thamm, R. Schirhagl, E. C. Langman, A. Schliesser, C. L. Degen, and A. Eichler, Membrane-based scanning force microscopy, *Phys. Rev. Applied* **15**, L021001 (2021).
- [11] R. Fischer, D. P. McNally, C. Reetz, G. G. T. Assumpção, T. Knief, Y. Lin, and C. A. Regal, Spin detection with a micromechanical trampoline: towards magnetic resonance microscopy harnessing cavity optomechanics, *New J. Phys.* **21**, 043049 (2019).
- [12] J. Kořata, O. Zilberberg, C. L. Degen, R. Chitra, and A. Eichler, Spin detection via parametric frequency conversion in a membrane resonator, *Phys. Rev. Applied* **14**, 014042 (2020).
- [13] T. M. Karg, B. Gouraud, C. T. Ngai, G.-L. Schmid, K. Hammerer, and P. Treutlein, Light-mediated strong coupling between a mechanical oscillator and atomic spins 1 meter apart, *Science* **369**, 174 (2020).
- [14] R. A. Thomas, M. Parniak, C. Østfeldt, C. B. Møller, C. Bærentsen, Y. Tsaturyan, A. Schliesser, J. Appel, E. Zeuthen, and E. S. Polzik, Entanglement between distant macroscopic mechanical and spin systems, *Nature Physics* **17**, 228 (2020).
- [15] M. A. Page, M. Goryachev, H. Miao, Y. Chen, Y. Ma, D. Mason, M. Rossi, C. D. Blair, L. Ju, D. G. Blair, A. Schliesser, M. E. Tobar, and C. Zhao, Gravitational wave detectors with broadband high frequency sensitivity, *Communications Physics* **4**, 10.1038/s42005-021-00526-2 (2021).
- [16] M. Yuan, M. A. Cohen, and G. A. Steele, Silicon nitride membrane resonators at millikelvin temperatures with quality factors exceeding 10^8 , *Applied Physics Letters* **107**, 263501 (2015).
- [17] R. Fischer, N. Kampel, G. Assumpção, P.-L. Yu, K. Cicak, R. Peterson, R. Simmonds, and C. Regal, Optical probing of mechanical loss of a Si-₃N-₄ membrane below 100 mK (2016), [arXiv:1611.00878](https://arxiv.org/abs/1611.00878).
- [18] Y. Seis, T. Capelle, E. Langman, S. Saarinen, E. Planz, and A. Schliesser, Ground state cooling of an ultracoherent electromechanical system (2021), [arXiv:2107.05552](https://arxiv.org/abs/2107.05552).
- [19] R. Kalra, A. Laucht, J. P. Dehollain, D. Bar, S. Freer, S. Simmons, J. T. Muhonen, and A. Morello, Vibration-induced electrical noise in a cryogen-free dilution refrigerator: Characterization, mitigation, and impact on qubit coherence, *Review of Scientific Instruments* **87**, 073905 (2016).
- [20] A. H. Ghadimi, D. J. Wilson, and T. J. Kippenberg, Radiation and internal loss engineering of high-stress silicon nitride nanobeams, *Nano Letters* **17**, 3501 (2017).
- [21] A. Beccari, D. A. Visani, S. A. Fedorov, M. J. Beryhi, V. Boureau, N. J. Engelsen, and T. J. Kippenberg, Strained crystalline nanomechanical resonators with quality factors above 10 billion, *Nature Physics* **18**, 436 (2022).
- [22] Y. Tao, J. M. Boss, B. A. Moores, and C. L. Degen, Single-crystal diamond nanomechanical resonators with quality factors exceeding one million, *Nature Communications* **5**, 10.1038/ncomms4638 (2014).
- [23] M. Héritier, A. Eichler, Y. Pan, U. Grob, I. Shorubalko, M. D. Krass, Y. Tao, and C. L. Degen, Nanoladder cantilevers made from diamond and silicon, *Nano Letters* **18**, 1814 (2018).
- [24] See supplemental material at [url will be inserted by publisher] for additional setup descriptions, more measurement data.

- [25] D. Rugar and P. Grütter, Mechanical parametric amplification and thermomechanical noise squeezing, *Phys. Rev. Lett.* **67**, 699 (1991).
- [26] S. A. Fedorov, N. J. Engelsen, A. H. Ghadimi, M. J. Breyhi, R. Schilling, D. J. Wilson, and T. J. Kippenberg, Generalized dissipation dilution in strained mechanical resonators, *Phys. Rev. B* **99**, 054107 (2019).
- [27] O. Maillet, D. Cattiaux, X. Zhou, R. R. Gazizulin, O. Bourgeois, A. D. Fefferman, and E. Collin, Nanomechanical damping via electron-assisted relaxation of two-level systems (2020), [arXiv:2009.03804](https://arxiv.org/abs/2009.03804) [[cond-mat.mes-hall](https://arxiv.org/abs/2009.03804)].
- [28] M. Aspelmeyer, T. J. Kippenberg, and F. Marquardt, Cavity optomechanics, *Rev. Mod. Phys.* **86**, 1391 (2014).
- [29] C. H. Metzger and K. Karrai, Cavity cooling of a microlever, *Nature* **432**, 1002 (2004).
- [30] C. Seoáñez, F. Guinea, and A. H. Castro Neto, Surface dissipation in nanoelectromechanical systems: Unified description with the standard tunneling model and effects of metallic electrodes, *Phys. Rev. B* **77**, 125107 (2008).
- [31] R. O. Behunin, F. Intravaia, and P. T. Rakich, Dimensional transformation of defect-induced noise, dissipation, and nonlinearity, *Physical Review B* **93**, 224110 (2016).
- [32] B. D. Hauer, P. H. Kim, C. Doolin, F. Souris, and J. P. Davis, Two-level system damping in a quasi-one-dimensional optomechanical resonator, *Physical Review B* **98**, 214303 (2018).
- [33] W. A. Phillips, Two-level states in glasses, *Reports on Progress in Physics* **50**, 1657 (1987).
- [34] G. J. Grabovskij, T. Peichl, J. Lisenfeld, G. Weiss, and A. V. Ustinov, Strain tuning of individual atomic tunneling systems detected by a superconducting qubit, *Science* **338**, 232 (2012).
- [35] G. Zolfagharkhani, A. Gaidarzhy, S.-B. Shim, R. L. Badzey, and P. Mohanty, Quantum friction in nanomechanical oscillators at millikelvin temperatures, *Physical Review B* **72**, 224101 (2005).
- [36] S. B. Shim, J. S. Chun, S. W. Kang, S. W. Cho, S. W. Cho, Y. D. Park, P. Mohanty, N. Kim, and J. Kim, Micromechanical resonators fabricated from lattice-matched and etch-selective GaAs/InGaP/GaAs heterostructures, *Applied Physics Letters* **91**, 133505 (2007).
- [37] M. Imboden and P. Mohanty, Evidence of universality in the dynamical response of micromechanical diamond resonators at millikelvin temperatures, *Phys. Rev. B* **79**, 125424 (2009).
- [38] K. J. Lulla, M. Defoort, C. Blanc, O. Bourgeois, and E. Collin, Evidence for the role of normal-state electrons in nanoelectromechanical damping mechanisms at very low temperatures, *Phys. Rev. Lett.* **110**, 177206 (2013).
- [39] M. Héri-tier, R. Pachlatko, Y. Tao, J. M. Abendroth, C. L. Degen, and A. Eichler, Spatial correlation between fluctuating and static fields over metal and dielectric substrates, *Phys. Rev. Lett.* **127**, 216101 (2021).
- [40] D. Martinez-Martin, R. Longuinhos, J. G. Izquierdo, A. Marele, S. S. Alexandre, M. Jaafar, J. M. Gómez-Rodríguez, L. Bañares, J. M. Soler, and J. Gomez-Herrero, Atmospheric contaminants on graphitic surfaces, *Carbon* **61**, 33 (2013).
- [41] P. R. Saulson, Thermal noise in mechanical experiments, *Physical Review D* **42**, 2437 (1990).
- [42] J. Moser, J. Güttinger, A. Eichler, M. J. Esplandiu, D. E. Liu, M. I. Dykman, and A. Bachtold, Ultrasensitive force detection with a nanotube mechanical resonator, *Nat. Nanotechnol.* **8**, 493 (2013).
- [43] S. L. de Bonis, C. Urgell, W. Yang, C. Samanta, A. Noury, J. Vergara-Cruz, Q. Dong, Y. Jin, and A. Bachtold, Ultrasensitive displacement noise measurement of carbon nanotube mechanical resonators, *Nano Letters* **18**, 5324 (2018).
- [44] M. Poggio and C. L. Degen, Force-detected nuclear magnetic resonance: Recent advances and future challenges, *Nanotechnology* **21**, 342001 (2010).
- [45] J. M. Nichol, T. R. Naibert, E. R. Hemesath, L. J. Lauhon, and R. Budakian, Nanoscale fourier-transform magnetic resonance imaging, *Phys. Rev. X* **3**, 031016 (2013).
- [46] U. Grob, M.-D. Krass, M. Héri-tier, R. Pachlatko, J. Rhensius, J. Kořata, B. A. J. Moores, H. Takahashi, A. Eichler, and C. L. Degen, Magnetic resonance force microscopy with a one-dimensional resolution of 0.9 nanometers, *Nano Lett.* **19**, 7935 (2019).
- [47] M. Rossi, D. Mason, J. Chen, Y. Tsaturyan, and A. Schliesser, Measurement-based quantum control of mechanical motion, *Nature* **563**, 53 (2018).
- [48] K. Y. Fong, W. H. P. Pernice, and H. X. Tang, Frequency and phase noise of ultrahigh Q silicon nitride nanomechanical resonators, *Phys. Rev. B* **85**, 161410(R) (2012).
- [49] R. Schilling, H. Schütz, A. H. Ghadimi, V. Sudhir, D. J. Wilson, and T. J. Kippenberg, Near-field integration of a SiN nanobeam and a SiO₂ microcavity for Heisenberg-limited displacement sensing, *Phys. Rev. Applied* **5**, 054019 (2016).
- [50] J. Guo, R. Norte, and S. Gröblacher, Feedback cooling of a room temperature mechanical oscillator close to its motional ground state, *Phys. Rev. Lett.* **123**, 223602 (2019).
- [51] D. J. Wilson, V. Sudhir, N. Piro, R. Schilling, A. Ghadimi, and T. J. Kippenberg, Measurement-based control of a mechanical oscillator at its thermal decoherence rate, *Nature* **524**, 325 (2015).
- [52] A. H. Ghadimi, *Ultra-coherent nano-mechanical resonators for quantum optomechanics at room temperature*, Tech. Rep. (EPFL, 2018).

Supplemental Material for: Soft-clamped silicon nitride string resonators at millikelvin temperatures

Thomas Gisler,¹ Mohamed Helal,¹ Deividas Sabonis,¹ Urs Grob,¹ Martin H eritier,¹ Christian L. Degen,¹ Amir H. Ghadimi,^{2,*} and Alexander Eichler^{1,†}

¹Laboratory for Solid State Physics, ETH Z urich, 8093 Z urich, Switzerland.

²Centre Suisse d'Electronique et de Microtechnique SA (CSEM), 2002 Neuch atel, Switzerland.

S1. OPTICAL FRINGES

Tuning the wavelength by changing the temperature of the laser diode allows to move within the optical fringe. For this we apply a voltage to the thermoelectric cooler (TEC) pins of the butterfly laser diode. While the motion of the string is encoded in the interference of the light reflected from the string resonator and the coated fiber end, the main fraction of the reflected light comes from the sample chip substrate, see Fig. S1(a). This results in the optical fringe shown in Fig. S1(b). Using a phase-lock loop (PLL) to drive and measure the displacement of the fundamental mode of the string - while sweeping the TEC voltage - reveals the position within the fringe where the largest signal is obtained. The TEC voltage sweep is performed for two different PLL setpoint phases shifted by π (orange and green in Fig. S1(b)). The mechanical signal is not maximized at the steepest slope of the optical fringe, as is typically observed with this interferometer setup [23]. Instead, the maximum position cannot be predicted from the fringe signal and must be measured directly as a function of the TEC voltage, as described above. The laser wavelength is then locked to this point using a PID feedback. This point corresponds to where the phase light reflected from the fiber end and the string are shifted by $\pm\pi$. The maxima of the orange and green signals correspond to maximum positive and negative optomechanical damping, respectively.

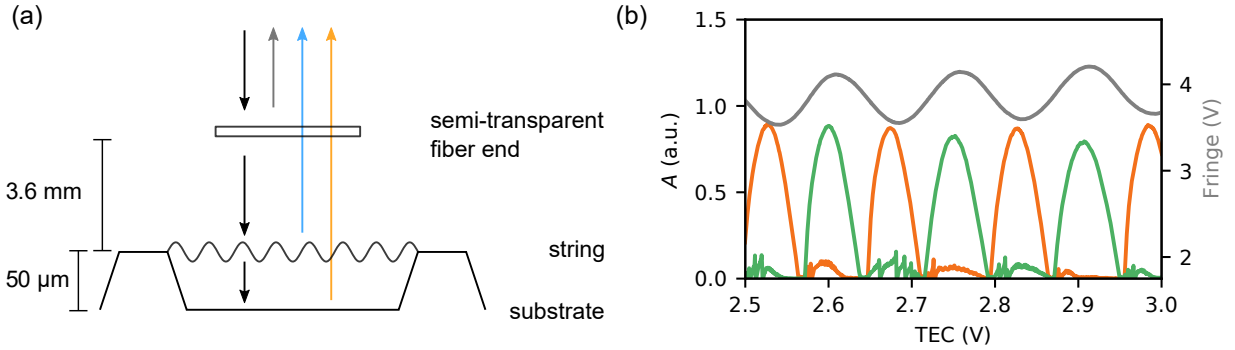


FIG. S1. **Interferometric detection method.** (a) Schematic of the optical interferometer, with light reflected from the fiber end (grey), the string (blue) and the substrate (orange). (b) Sweeping the TEC voltage (corresponds to laser wavelength) and measuring the optical fringe (grey - right y-axis) and the amplitude of the fundamental mode with two different PLL setpoint phases ϕ_{PLL} (orange: $\phi_{\text{PLL}} = \phi_0$, green: $\phi_{\text{PLL}} = \phi_0 + \pi$, left y-axis).

* Corresponding author: amir.ghadimi@csem.ch

† Corresponding author: eichlera@ethz.ch

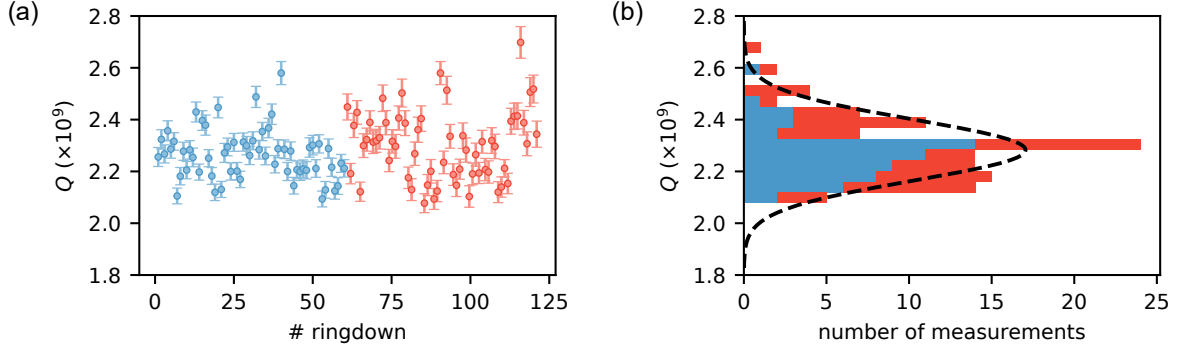


FIG. S2. **Repeatability of measured Q .** Repetition of ringdown measurements with $t_{\text{on}} = 5$ s for two different “laser off” periods ($t_{\text{off}}^{\text{blue}} = 150$ s and $t_{\text{off}}^{\text{red}} = 250$ s). (a) Measured Q and (b) histogram of these values together with a Gaussian fit with mean value 2.282×10^9 and standard deviation 0.116×10^9 .

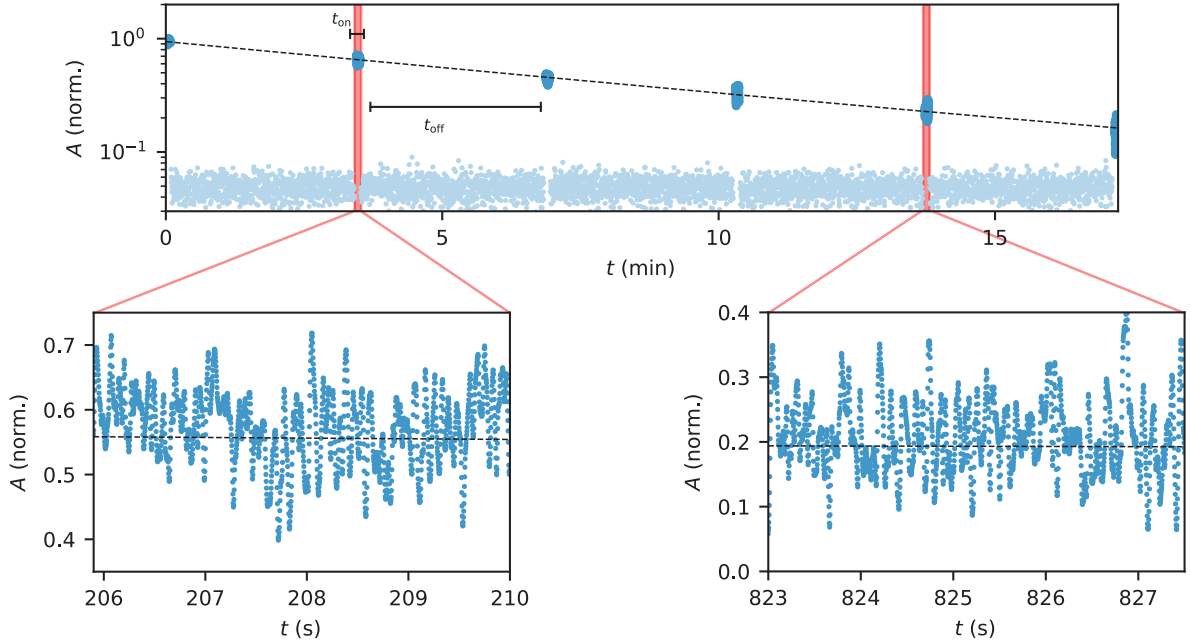


FIG. S3. **Zoom ringdown** The same ringdown as in Fig. 1(c) presented with zoomed details. The large spread of data points is due to detector noise.

S2. REPEATABILITY OF RINGDOWN MEASUREMENTS

In order to verify the measured Q we repeatedly conducted ringdown measurements with the same settings. In Fig. S2(a-b) we collect the extracted Q values of the localized mode for $t_{\text{off}} = 150$ s and 250 s of device B at $T_{\text{plate}} = 48$ mK and $t_{\text{on}} = 5$ s. The mean of the measured values is 2.282×10^9 with a standard deviation of 0.116×10^9 . This mean value for Q is used to calculate the intrinsic force sensitivity and thermal decoherence time in the main text. The zoomed data in Fig. S3 demonstrate the large spread of data points due to the low-pass filtered detector noise.

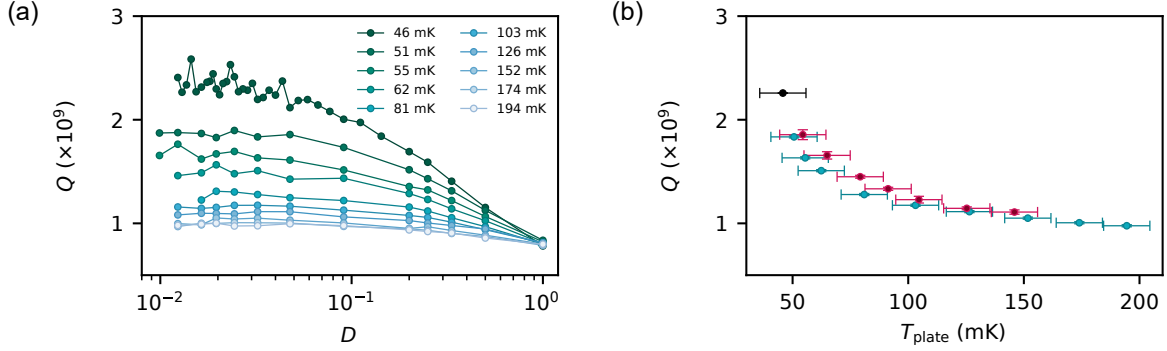


FIG. S4. **Comparing the different heaters.** (a) Driven PEA with frequency 1.5 MHz with driving amplitudes between 50 mV and 200 mV. The temperatures in the legend correspond to T_{plate} . Note that the top line, corresponding to the unheated string, is identical to the measurement in the main text. (b) Comparison of Q as a function of T_{plate} for the two heaters (blue closer to the sample than purple).

S3. VARIABLE TEMPERATURE MEASUREMENTS

We used two different heaters to locally change the temperature of the nanomechanical resonator. For each temperature T_{plate} (extracted from the mixing chamber temperature, see Fig. S5) we extracted Q for different duty cycles D . In the main text, data are shown for a resistive heater mounted a few centimeters from the sample on the sample plate. In Fig. S4(a) we supply the results for the second heater, consisting of the piezoelectric actuator (PEA) mounted closer to the string chip. Here, a temperature variation was induced by applying a high-frequency signal $f_{\text{heat}} = 1.5 \text{ MHz}$ to the PEA, carefully avoiding any mechanical resonance frequency. In Fig. S4(b) we compare the results of the two heating methods and obtain very similar Q values.

S4. CALIBRATION OF SAMPLE PLATE TEMPERATURE

During the measurements presented in the main text, the thermometer mounted on the sample plate could not be used due to a wiring problem. We later repeated the cooldown (without a mechanical resonator device) to calibrate the temperature difference between the mixing chamber plate and the sample plate. All temperatures in the main text are stated after the conversion using the calibration measurement shown in Fig. S5. We infer a base temperature of 41 mK on the sample plate with a systematic uncertainty of 10 mK stemming from the sensor calibration. The measurement was performed with a lock-in amplifier at a bias current of roughly 1 nA applied with a local oscillator frequency of 33 Hz. The power dissipated over the temperature sensor was below 1 pW.

S5. SILICON NITRIDE STRINGS

A. Fabrication

The devices used in this work were designed and fabricated at CSEM based on the previous work by authors [6, 52]. Briefly, the fabrication process flow starts with a low-pressure chemical vapor deposition (LPCVD) of high-stress

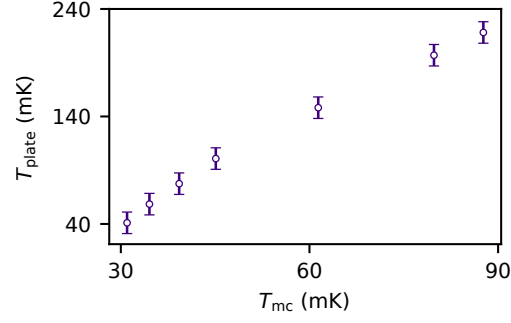


FIG. S5. **Calibration of sample plate temperature.** Sample plate temperature T_{plate} as function of the mixing chamber temperature T_{mc} for variable power delivered to a heater on the sample plate. The error bars correspond to the calibration uncertainty (10 mK) of the RuO_2 sensor.

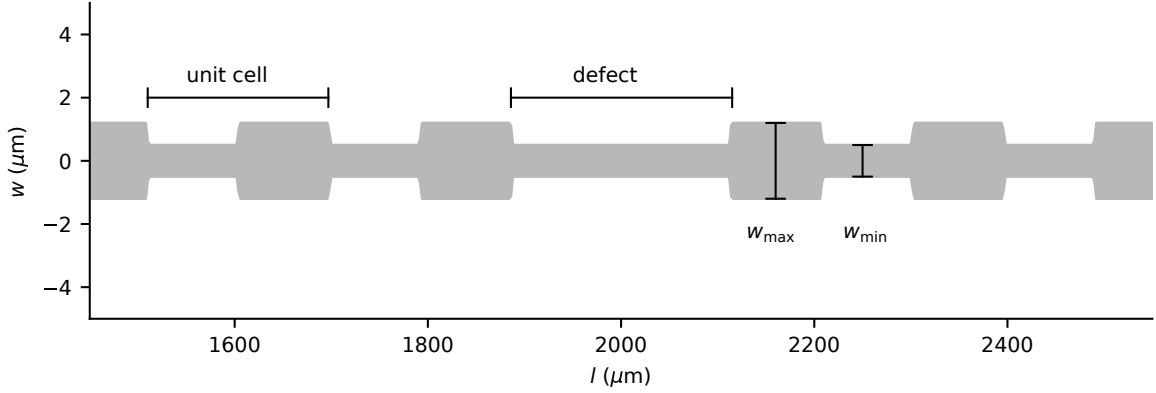


FIG. S6. **Nanostring geometry.** Geometrical shape of the silicon nitride string with $w_{min} = 500$ nm and $w_{max} = 1200$ nm and a length of 4 mm.

Si_3N_4 on a Si substrate. This is followed by electron beam (ebeam) lithography of the corrugated string geometry on top of Si_3N_4 layer using a flowable oxide (FOX-16 $\text{\textcircled{R}}$) resist (2). Structures are then transferred to the Si_3N_4 layer by reactive ion etching (RIE). Finally, the mechanical beams are released from the underlying Si substrate in potassium hydroxide (KOH) bath and drying using a critical point dryer (CPD). The complete process flow is considerably more complex and includes several intermediate steps to ensure the prevention of collapsing of released nanobeams due to their extreme aspect ratios. The detailed process flow can be found in [6, 52].

B. Geometrical shape of strings

In this work, we used different corrugated Si_3N_4 strings with similar geometries. Figure S6 shows the area around the defect in the center of such a string. Device B and C have the same thickness, size and number of unit cell but their defect-to-unit-cell ratio differs (Device B 1.1 and device C 1.2).

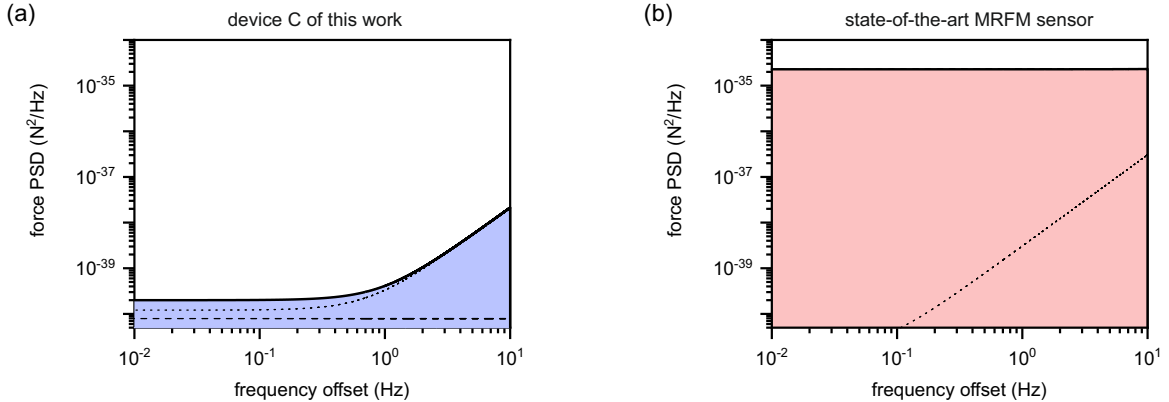


FIG. S7. **Force sensitivity comparison as a function of the detuning from the resonance frequency f_0 .** (a) Estimated contributions to the force noise power spectral density of device C measured in this work at a conservative temperature of 80 mK. We assume that an on-chip cavity readout can reach a displacement sensitivity of $2 \times 10^{-28} \text{ m}^2 \text{ Hz}^{-1}$ without significant additional heating [49, 50]. For the magnetic field gradient produced by a coated AFM tip at a distance of 10 to 30 nm, we use a conservative value of $1 \times 10^7 \text{ T m}^{-1}$. (b) Cantilever device used in state-of-the-art NanoMRI measurements with a mass of $1 \times 10^{-13} \text{ pg}$, a resonance frequency of 3.5 kHz and a quality factor of 25000, (manuscript in preparation, similar performance as in Ref. [46]). This sensor is operated at 4.7 K and no on-chip cavity readout is possible in the present setup, limiting the displacement sensitivity to $4 \times 10^{-24} \text{ m}^2 \text{ Hz}^{-1}$. The magnetic field gradient produced by the nanomagnet in this experiment was found to have a maximum value of $2.8 \times 10^6 \text{ T m}^{-1}$. In both panels, a dashed black line is the thermal noise (including the zero-point fluctuations), a dotted black line is the sum of quantum back-action and detector noise, and a thick black line and the colored area indicate the total force noise. The noise of the cantilever device in (b) is dominated by the thermomechanical noise contribution, such that the solid and dashed black lines overlap.

C. Force noise evaluation for nanoscale MRI

The devices used in this work are promising candidates for force sensing in the zeptonewton range. Such a force sensitivity is crucial, for instance, for nanoscale magnetic resonance microscopy (NanoMRI) and for coherent spin-mechanics coupling. In Fig. S7, we compare the predicted performance of device C measured in this work with a state-of-the-art cantilever sensor used for our most recent NanoMRI demonstration [?], which is comparable to that used in previous experiments [46]. The only modification that we additionally assume for the string device in Fig. S7(a) is the implementation of an on-chip cavity readout with a displacement sensitivity of $2 \times 10^{-28} \text{ m}^2 \text{ Hz}^{-1}$, as discussed in the main text [49, 50]. For a bandwidth of 1 Hz, the present string device has a total force noise standard deviation of $1.7 \times 10^{-20} \text{ N}$, corresponding to the force generated by 0.01 hydrogen atoms in the magnetic field gradient predicted from finite element calculations. The cantilever device in Fig. S7(b) achieves a force noise standard deviation of $3.4 \times 10^{-18} \text{ N}$ in the same bandwidth, resulting in a theoretical sensitivity of roughly 7400 hydrogen atoms. The string resonator is therefore expected to produce highly superior results, allowing the detection of the forces generated by individual nuclei.

-
- [1] S. S. Verbridge, H. G. Craighead, and J. M. Parpia, A megahertz nanomechanical resonator with room temperature quality factor over a million, *Applied Physics Letters* **92**, 013112 (2008).
 - [2] G. Anetsberger, E. Gavartin, O. Arcizet, Q. P. Unterreithmeier, E. M. Weig, M. L. Gorodetsky, J. P. Kotthaus, and T. J. Kippenberg, Measuring nanomechanical motion with an imprecision below the standard quantum limit, *Phys. Rev. A* **82**,

- 061804(R) (2010).
- [3] C. Reetz, R. Fischer, G. Assumpção, D. McNally, P. Burns, J. Sankey, and C. Regal, Analysis of membrane phononic crystals with wide band gaps and low-mass defects, *Physical Review Applied* **12**, 044027 (2019).
 - [4] C. Reinhardt, T. Müller, A. Bourassa, and J. C. Sankey, Ultralow-noise sin trampoline resonators for sensing and optomechanics, *Phys. Rev. X* **6**, 021001 (2016).
 - [5] Y. Tsaturyan, A. Barg, E. S. Polzik, and A. Schliesser, Ultracoherent nanomechanical resonators via soft clamping and dissipation dilution, *Nature Nanotechnology* **12**, 776 (2017).
 - [6] A. H. Ghadimi, S. A. Fedorov, N. J. Engelsen, M. J. Beryhi, R. Schilling, D. J. Wilson, and T. J. Kippenberg, Elastic strain engineering for ultralow mechanical dissipation, *Science* **360**, 764 (2018).
 - [7] A. Beccari, M. J. Beryhi, R. Groth, S. A. Fedorov, A. Arabmoheghi, N. J. Engelsen, and T. J. Kippenberg, Hierarchical tensile structures with ultralow mechanical dissipation (2021), [arXiv:2103.09785](https://arxiv.org/abs/2103.09785).
 - [8] T. Bağcı, A. Simonsen, S. Schmid, L. G. Villanueva, E. Zeuthen, J. Appel, J. M. Taylor, A. Sørensen, K. Usami, A. Schliesser, and E. S. Polzik, Optical detection of radio waves through a nanomechanical transducer, *Nature* **507**, 81 (2014).
 - [9] R. W. Andrews, R. W. Peterson, T. P. Purdy, K. Cicak, R. W. Simmonds, C. A. Regal, and K. W. Lehnert, Bidirectional and efficient conversion between microwave and optical light, *Nature Physics* **10**, 321 (2014).
 - [10] D. Hälgl, T. Gisler, Y. Tsaturyan, L. Catalini, U. Grob, M.-D. Krass, M. Hérítier, H. Mattiat, A.-K. Thamm, R. Schirhagl, E. C. Langman, A. Schliesser, C. L. Degen, and A. Eichler, Membrane-based scanning force microscopy, *Phys. Rev. Applied* **15**, L021001 (2021).
 - [11] R. Fischer, D. P. McNally, C. Reetz, G. G. T. Assumpção, T. Knief, Y. Lin, and C. A. Regal, Spin detection with a micromechanical trampoline: towards magnetic resonance microscopy harnessing cavity optomechanics, *New J. Phys.* **21**, 043049 (2019).
 - [12] J. Kořata, O. Zilberberg, C. L. Degen, R. Chitra, and A. Eichler, Spin detection via parametric frequency conversion in a membrane resonator, *Phys. Rev. Applied* **14**, 014042 (2020).
 - [13] T. M. Karg, B. Gouraud, C. T. Ngai, G.-L. Schmid, K. Hammerer, and P. Treutlein, Light-mediated strong coupling between a mechanical oscillator and atomic spins 1 meter apart, *Science* **369**, 174 (2020).
 - [14] R. A. Thomas, M. Parniak, C. Østfeldt, C. B. Møller, C. Bærentsen, Y. Tsaturyan, A. Schliesser, J. Appel, E. Zeuthen, and E. S. Polzik, Entanglement between distant macroscopic mechanical and spin systems, *Nature Physics* **17**, 228 (2020).
 - [15] M. A. Page, M. Goryachev, H. Miao, Y. Chen, Y. Ma, D. Mason, M. Rossi, C. D. Blair, L. Ju, D. G. Blair, A. Schliesser, M. E. Tobar, and C. Zhao, Gravitational wave detectors with broadband high frequency sensitivity, *Communications Physics* **4**, 10.1038/s42005-021-00526-2 (2021).
 - [16] M. Yuan, M. A. Cohen, and G. A. Steele, Silicon nitride membrane resonators at millikelvin temperatures with quality factors exceeding 10^8 , *Applied Physics Letters* **107**, 263501 (2015).
 - [17] R. Fischer, N. Kampel, G. Assumpção, P.-L. Yu, K. Cicak, R. Peterson, R. Simmonds, and C. Regal, Optical probing of mechanical loss of a Si₃N₄ membrane below 100 mK (2016), [arXiv:1611.00878](https://arxiv.org/abs/1611.00878).
 - [18] Y. Seis, T. Capelle, E. Langman, S. Saarinen, E. Planz, and A. Schliesser, Ground state cooling of an ultracoherent electromechanical system (2021), [arXiv:2107.05552](https://arxiv.org/abs/2107.05552).
 - [19] R. Kalra, A. Laucht, J. P. Dehollain, D. Bar, S. Freer, S. Simmons, J. T. Muhonen, and A. Morello, Vibration-induced electrical noise in a cryogen-free dilution refrigerator: Characterization, mitigation, and impact on qubit coherence, *Review of Scientific Instruments* **87**, 073905 (2016).
 - [20] A. H. Ghadimi, D. J. Wilson, and T. J. Kippenberg, Radiation and internal loss engineering of high-stress silicon nitride nanobeams, *Nano Letters* **17**, 3501 (2017).

- [21] A. Beccari, D. A. Visani, S. A. Fedorov, M. J. Beryhi, V. Boureau, N. J. Engelsen, and T. J. Kippenberg, Strained crystalline nanomechanical resonators with quality factors above 10 billion, *Nature Physics* **18**, 436 (2022).
- [22] Y. Tao, J. M. Boss, B. A. Moores, and C. L. Degen, Single-crystal diamond nanomechanical resonators with quality factors exceeding one million, *Nature Communications* **5**, 10.1038/ncomms4638 (2014).
- [23] M. H eritier, A. Eichler, Y. Pan, U. Grob, I. Shorubalko, M. D. Krass, Y. Tao, and C. L. Degen, Nanoladder cantilevers made from diamond and silicon, *Nano Letters* **18**, 1814 (2018).
- [24] See supplemental material at [url will be inserted by publisher] for additional setup descriptions, more measurement data.
- [25] D. Rugar and P. Gr utter, Mechanical parametric amplification and thermomechanical noise squeezing, *Phys. Rev. Lett.* **67**, 699 (1991).
- [26] S. A. Fedorov, N. J. Engelsen, A. H. Ghadimi, M. J. Beryhi, R. Schilling, D. J. Wilson, and T. J. Kippenberg, Generalized dissipation dilution in strained mechanical resonators, *Phys. Rev. B* **99**, 054107 (2019).
- [27] O. Maillet, D. Cattiaux, X. Zhou, R. R. Gazizulin, O. Bourgeois, A. D. Fefferman, and E. Collin, Nanomechanical damping via electron-assisted relaxation of two-level systems (2020), [arXiv:2009.03804 \[cond-mat.mes-hall\]](https://arxiv.org/abs/2009.03804).
- [28] M. Aspelmeyer, T. J. Kippenberg, and F. Marquardt, Cavity optomechanics, *Rev. Mod. Phys.* **86**, 1391 (2014).
- [29] C. H. Metzger and K. Karrai, Cavity cooling of a microlever, *Nature* **432**, 1002 (2004).
- [30] C. Seo anez, F. Guinea, and A. H. Castro Neto, Surface dissipation in nanoelectromechanical systems: Unified description with the standard tunneling model and effects of metallic electrodes, *Phys. Rev. B* **77**, 125107 (2008).
- [31] R. O. Behunin, F. Intravaia, and P. T. Rakich, Dimensional transformation of defect-induced noise, dissipation, and nonlinearity, *Physical Review B* **93**, 224110 (2016).
- [32] B. D. Hauer, P. H. Kim, C. Doolin, F. Souris, and J. P. Davis, Two-level system damping in a quasi-one-dimensional optomechanical resonator, *Physical Review B* **98**, 214303 (2018).
- [33] W. A. Phillips, Two-level states in glasses, *Reports on Progress in Physics* **50**, 1657 (1987).
- [34] G. J. Grabovskij, T. Peichl, J. Lisenfeld, G. Weiss, and A. V. Ustinov, Strain tuning of individual atomic tunneling systems detected by a superconducting qubit, *Science* **338**, 232 (2012).
- [35] G. Zolfagharkhani, A. Gaidarzhy, S.-B. Shim, R. L. Badzey, and P. Mohanty, Quantum friction in nanomechanical oscillators at millikelvin temperatures, *Physical Review B* **72**, 224101 (2005).
- [36] S. B. Shim, J. S. Chun, S. W. Kang, S. W. Cho, S. W. Cho, Y. D. Park, P. Mohanty, N. Kim, and J. Kim, Micromechanical resonators fabricated from lattice-matched and etch-selective GaAs/InGaP/GaAs heterostructures, *Applied Physics Letters* **91**, 133505 (2007).
- [37] M. Imboden and P. Mohanty, Evidence of universality in the dynamical response of micromechanical diamond resonators at millikelvin temperatures, *Phys. Rev. B* **79**, 125424 (2009).
- [38] K. J. Lulla, M. Defoort, C. Blanc, O. Bourgeois, and E. Collin, Evidence for the role of normal-state electrons in nanoelectromechanical damping mechanisms at very low temperatures, *Phys. Rev. Lett.* **110**, 177206 (2013).
- [39] M. H eritier, R. Pachlatko, Y. Tao, J. M. Abendroth, C. L. Degen, and A. Eichler, Spatial correlation between fluctuating and static fields over metal and dielectric substrates, *Phys. Rev. Lett.* **127**, 216101 (2021).
- [40] D. Martinez-Martin, R. Longuinhos, J. G. Izquierdo, A. Marele, S. S. Alexandre, M. Jaafar, J. M. G omez-Rodr iguez, L. Ba nares, J. M. Soler, and J. Gomez-Herrero, Atmospheric contaminants on graphitic surfaces, *Carbon* **61**, 33 (2013).
- [41] P. R. Saulson, Thermal noise in mechanical experiments, *Physical Review D* **42**, 2437 (1990).
- [42] J. Moser, J. G uttinger, A. Eichler, M. J. Esplandi u, D. E. Liu, M. I. Dykman, and A. Bachtold, Ultrasensitive force detection with a nanotube mechanical resonator, *Nat. Nanotechnol.* **8**, 493 (2013).
- [43] S. L. de Bonis, C. Urgell, W. Yang, C. Samanta, A. Noury, J. Vergara-Cruz, Q. Dong, Y. Jin, and A. Bachtold, Ultrasensitive displacement noise measurement of carbon nanotube mechanical resonators, *Nano Letters* **18**, 5324 (2018).

- [44] M. Poggio and C. L. Degen, Force-detected nuclear magnetic resonance: Recent advances and future challenges, [Nanotechnology](#) **21**, 342001 (2010).
- [45] J. M. Nichol, T. R. Naibert, E. R. Hemesath, L. J. Lauhon, and R. Budakian, Nanoscale fourier-transform magnetic resonance imaging, [Phys. Rev. X](#) **3**, 031016 (2013).
- [46] U. Grob, M.-D. Krass, M. H eritier, R. Pachlatko, J. Rhensius, J. Kořata, B. A. J. Moores, H. Takahashi, A. Eichler, and C. L. Degen, Magnetic resonance force microscopy with a one-dimensional resolution of 0.9 nanometers, [Nano Lett.](#) **19**, 7935 (2019).
- [47] M. Rossi, D. Mason, J. Chen, Y. Tsaturyan, and A. Schliesser, Measurement-based quantum control of mechanical motion, [Nature](#) **563**, 53 (2018).
- [48] K. Y. Fong, W. H. P. Pernice, and H. X. Tang, Frequency and phase noise of ultrahigh Q silicon nitride nanomechanical resonators, [Phys. Rev. B](#) **85**, 161410(R) (2012).
- [49] R. Schilling, H. Sch utz, A. H. Ghadimi, V. Sudhir, D. J. Wilson, and T. J. Kippenberg, Near-field integration of a SiN nanobeam and a SiO₂ microcavity for Heisenberg-limited displacement sensing, [Phys. Rev. Applied](#) **5**, 054019 (2016).
- [50] J. Guo, R. Norte, and S. Gr oblacher, Feedback cooling of a room temperature mechanical oscillator close to its motional ground state, [Phys. Rev. Lett.](#) **123**, 223602 (2019).
- [51] D. J. Wilson, V. Sudhir, N. Piro, R. Schilling, A. Ghadimi, and T. J. Kippenberg, Measurement-based control of a mechanical oscillator at its thermal decoherence rate, [Nature](#) **524**, 325 (2015).
- [52] A. H. Ghadimi, *Ultra-coherent nano-mechanical resonators for quantum optomechanics at room temperature*, Tech. Rep. (EPFL, 2018).